International Journal of Mechanical Engineering and Applications
2022; 10(6): 144-159
http://www.sciencepublishinggroup.com/j/ijmea
doi: 10.11648/j.ijmea.20221006.13
ISSN: 2330-023X (Print); ISSN: 2330-0248 (Online)

Characteristic Analysis of Two Pairing Origami Polyhedrons and Their Application to Beverage Containers

Aya Abe*, Ichiro Hagiwara, Yang Yang, Chie Nara

Meiji Institute for Advanced Study of Mathematical Sciences, Meiji University, Tokyo, Japan

Email address:

aya_abe@meiji.ac.jp (Aya Abe), ihagi@meiji.ac.jp (Ichiro Hagiwara), piscesyy0227@gmail.com (Yang Yang), cnara@jeans.ocn.ne.jp (Chie Nara)

*Corresponding author

To cite this article:

Aya Abe, Ichiro Hagiwara, Yang Yang, Chie Nara. Characteristic Analysis of Two Pairing Origami Polyhedrons and Their Application to Beverage Containers. *International Journal of Mechanical Engineering and Applications*. Vol. 10, No. 6, 2022, pp. 144-159.
doi: 10.11648/j.ijmea.20221006.13

Received: November 2, 2022; **Accepted**: November 21, 2022; **Published**: November 29, 2022

Abstract: Producing industrial goods with origami structure, such as cans or bottles which can be folded neatly after drinking up, is an idea anyone could easily think of. However, this idea has not been put in practical use yet. Recently, Tachi-Miura polyhedron (TMP) is gaining attention as a 3-dimensional version of Miura-Ori. Meanwhile, Nojima Polyhedron (NP) has been found to be similar as TMP and it is considered that both are able to be analyzed from the point of pairing origami structures proposed by Nojima. The pairing origami is generated by sticking the symmetry 2-dimensional parts to each other to create 3-dimensional shapes. In this study, NP and TMP are focused on and the possibility of the idea is examined. NP which is a mirror symmetry structure and TMP which is a glide symmetry structure, both can be folded not only in the axial but also in the radial direction, and so it would be convenient if they can be applied to beverage containers. In this study, whether both structures are rigid folding or not is investigated geometrically, and then how this gives influence on the energy absorbing characteristics is considered quantically. In the generation of the model, since NP is not rigid folding, a model with accurate coordinates cannot be established because deformation occurs on the surface at the folding stage, so the coordinates are determined by approximation. On the other hand, in the case of TMP, the coordinates of each point can be accurately indicated by parameters, so a model with accurate coordinates is established. Moreover, an engineering possibility to apply both structures in beverage containers is explored by studying their crushing characteristics on simulation. As a result, whether a rigid folding or not has some influence on its deformation mode, however it is shown that it has no influence on the purpose to investigate its possibility for industrialization. This is the first step to make sure the effective usages of the foldable pairing origami structure.

Keywords: Origami Engineering, Energy Absorption Property, Rigid Folding, 4 Folding Lines Type, 6 Folding Lines Type, Reversed Spiral Origami Structure, Nojima Polyhedron, Tachi-Miura Polyhedron

1. Introduction

In recent years, origami engineering has received much attention and many related papers have been published. In general, the origami structure has 2 major features: light but stiff and deployable. Therefore, in the industrial world, they utilize one of these features, light but stiff, such as in honeycombs and octet truss structures [1-3].

As far as the deployable feature, there are many researches such as space structures [4–8], robot arm [9], waterbomb [10] and splendid metamaterials [11]. Here the energy absorption properties of origami structures with deployable features are discussed. There are also many researches concerned with energy absorption of origami structure here discussed. There are 2 types of researches in energy absorption problems where one is to maximize energy absorption as much as possible like vehicle crash problem and another is to minimize the maximum load as small as possible like crush problem of beverage can. As far as the former one, Xiang et al. introduce mainly 4 research groups [12] led by Lu and Chen [13], You [14-16], Wang [17, 18] and Xie [19, 20]. All

of them use 4 folding lines type "Bellows Fold" which has 4 folding lines at every intersection. On the other hand, Hagiwara and collaborators treat 6 folding lines type "Reversed Spiral Origami Structure (RSO) [21-23]" which has 6 ones at every intersection.

Anyway, forming methods, which is not expensive, for industrialization with 2 types of origami structures have not been obtained. But recently, Zhao et al. have developed a 6-folding type "Reversed Torsional Origami Structure (RTO)" method which is very cheaply by partial-heating torsion forming method [24].

As far as the latter one, if it is possible to fold empty cans and Polyethylene Terephthalate (PET) bottles after drinking, new industrialization will be possible. Some researchers have attempted to put this industrialization in practical use. For example, Nojima has tried to obtain such PET bottles using his invented RSO [25]. Kamata et al. [26] and Ario [27] have also tried to apply the RSO to foldable PET bottles. However, none of them succeeded in practical use mainly because spring back caused it to return to its original height even if it was successfully folded. Recently Hagiwara et al. have succeeded to solve this problem with 6 folding lines type origami structure RSO [28]. And so, it is expected for practical use. In such a way, it has been obtained expectable results with 6 folding origami structures for crush energy absorption with RTO and for foldable pet bottle with RSO. Before full-scale industrialization of these, the possibilities of foldable can using pairing origami proposed by Nojima [29, 30] should be considered.

Recently, Tachi-Miura polyhedron [31] is gaining attention as a 3-dimensional version of Miura-Ori. Meanwhile, Nojima Polyhedron has been found to be similar as Tachi-Miura Polyhedron and it is considered that both are able to be analyzed from the point of pairing origami structures. Both Polyhedrons can be folded not only in the vertical direction but also in the radial direction. Here, the applicability of the pairing origami structures to foldable cans is studied. It is believed that this study is useful because these structures can basically be produced at low cost by accordion type folding. In chapter 2, it is reviewed that the pairing origami structures and the geometrical features of Nojima polyhedron and Tachi-Miura polyhedron are examined, then it is described that the difference between them in terms of rigid folding. In addition, the production methods for these two structures from the viewpoint of the origami engineering method currently developed is described. In chapter 3, it is considered that formulations for obtaining the coordinates of the nodes necessary for model creation and formulations that always hold between folding angles in any folding state in each method. In chapter 4, an optimal analysis is performed to reduce the force required at the time of crushing by the finite element method (FEM) for the aluminum can model created by pairing origami method. And why these two polyhedrons are less likely to bend during crushing is explained. In chapter 5, the feasibility of application of pairing origami to aluminum cans is considered.

2. Nojima and Tachi-Miura Polyhedrons

2.1. Pairing Origami

Since pairing origami is described in detail in some research, the outline of this is explained here [28, 29]. Pairing origami is generated by sticking the symmetry 2-dimensional parts to each other to create 3-dimensional shapes. The condition of fold is automatically held in the pairing part. And, in symmetric pairing origami, basically, in the case of one unit of polyhedron, as shown in Figure 1(a), the patterns of Miura-Ori are arranged symmetrically, and they are laminated as shown in (b). When one unit of polyhedron is joined together, it becomes as (c) and it can fold in zigzag as shown in (d). In this study, the Nojima Polyhedron and the Tachi-Miura Polyhedron are considered from the viewpoint of the pairing origami.

2.2. Geometrical Characteristics of Nojima and Tachi-Miura Polyhedrons

Table 1. shows the geometrical characteristics of Nojima Polyhedron (NP) and Tachi-Miura Polyhedron (TMP) as described in some research [32, 33]. NP has one hinge at the pairing part, while TMP has 2 hinges. NP is mirror symmetry which sticks together 2 origami parts which are the same exactly. TMP is glide symmetry which sticks together 2 origami parts which are not the same exactly but staggered one by one to face each other.

The most characteristic difference between NP and TMP is that the relationship between the angles α and β. In NP, it is $\beta = 2\alpha$ as shown in Figure 3(a). In TMP, that is $\beta = \alpha$ as shown in Figure 4(a).

Figure 2 shows the crease patterns and the folding process of both Polyhedrons. If they are folded according to folding lines and pasted together, it is possible to fold them in both the horizontal and the vertical directions. The solid lines and the dashed lines indicate the mountain fold lines and the valley fold lines respectively. Figure 3(a) shows the unit components of NP. In the state of (b) in which the shape is slightly formed into a 3-dimensional shape, the parameter is defined with the half angle of the dihedral angle θ as shown in the figure. As the folding state changes, θ changes from 0° to 90° and $2\alpha - \delta$ changes from 2α to 0° (δ changes from 0° to 2α). Similarly, Figure 4(a) shows the unit component of TMP. Again, in the state (b) in which the shape is slightly formed into a 3-dimensional shape, the parameter is defined with the half angle of the dihedral angle θ. As θ changes from 0° to 90°, $2\alpha - \delta$ changes from 2α to 0° (δ changes from 0° to 2α). Both NP and TMP have relationships of angles in the respective states as shown in Table 2.

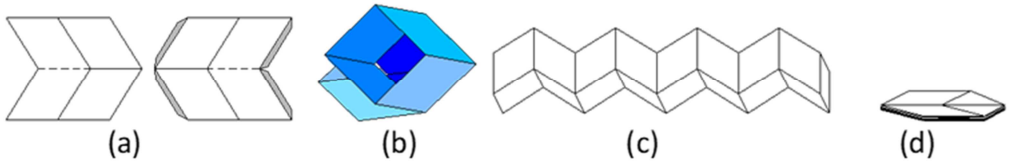

Figure 1. *Pairing origami structure. (a) Minimum unit development of symmetry pairing origami; (b) Pasted together model of (a); (c) Model of connected minimum units; (d) Model from folded (c).*

Table 1. *Geometrical characteristics of NP and TMP.*

	NP	**TMP**
Composed of	2 sheets	2 sheets
Parameters	d, l, m, α, θ, N β = 2α	d, l, m, α, θ, N β = α
Pairing region	Single hinge	Double hinge
Main region	Mountain lines: 16 Valley lines: 10 V-M-V / V-M-V or M-V-M / M-V-M	Mountain lines: 17 Valley lines: 9 M-V-M / V-M-V or V-M-V / M-V-M
Symmetry	Mirror symmetry	Glide symmetry

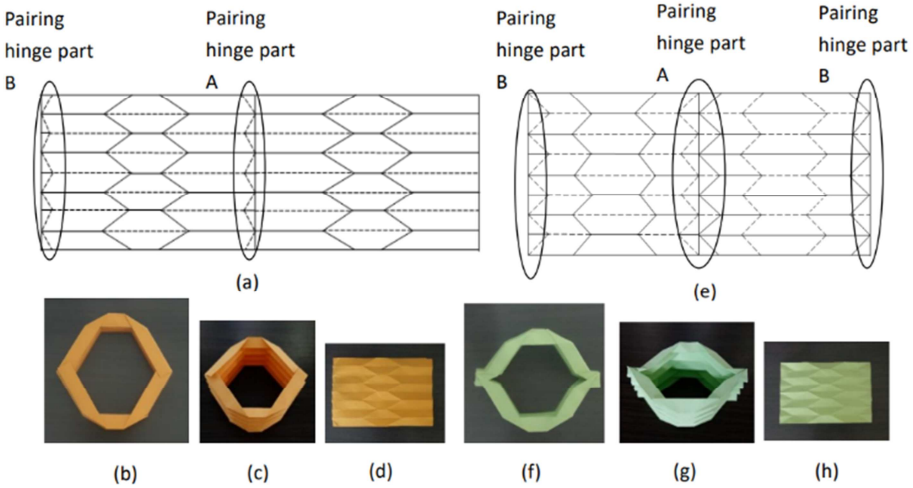

Figure 2. *The folding process of origami structures. (a) The crease pattern of NP; (b) The vertically flat folded NP from top; (c) The 3D shape of NP from diagonally above; (d) The horizontally flat folded NP from side; (e) The crease pattern of TMP; (f) The vertically flat folded TMP from top; (g) The 3D shape of TMP from diagonally above; (h) The horizontally flat folded TMP from side; Solid lines: mountain fold, dotted lines: valley fold.*

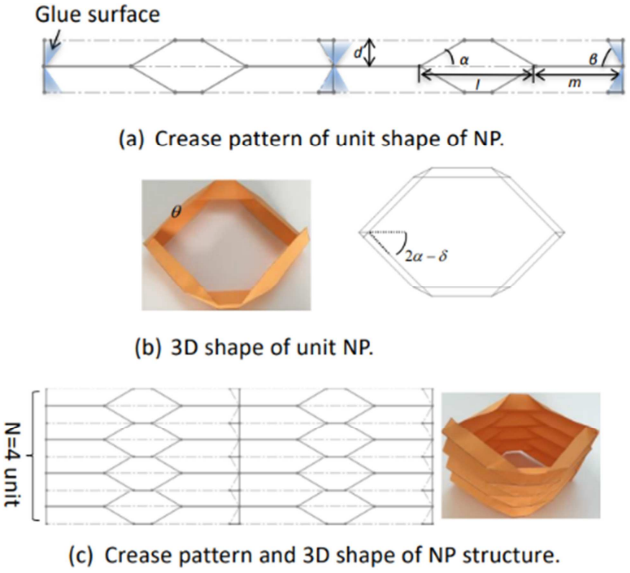

Figure 3. *The geometric characteristics of NP (a)~(c).*

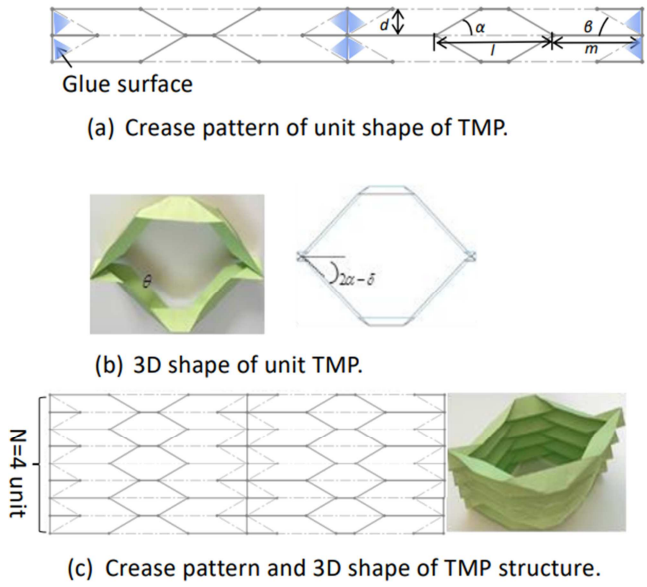

Figure 4. *The geometric characteristics of TMP (a)~(c).*

Table 2. *Relationships between each angle.*

	Folded horizontally	**In between**	**Folded vertically**
Dihedral angle	0°	90°	180°
θ	0°	45°	90°
2α-δ	2α	α	0°
δ	0°	α	2α

2.3. Comparison of Nojima and Tachi-Miura Polyhedrons from the Viewpoint of Rigid Folding

Next, both Polyhedrons are compared qualitatively from geometric points of view, regardless of whether they are rigid folding or not. Tachi-Miura Polyhedron is rigid folding. Figure 5(a) shows one unit of the crease pattern of TMP. The parts in light blue are the gluing parts. When folded, the line segment A_1B_1 coincides with the line segment A_7B_8. 2 parallelograms $A_1B_2B_3A_2$ and $A_5B_7B_8A_6$ which are adjacent to each other with a pairing part in between are focused on and their movements are observed.

In TMP, each one side of 2 adjacent parallelograms is one side of a hinge. In parallelogram $A_1B_2B_3A_2$, it corresponds to side A_1B_2, while in parallelogram $A_5B_7B_8A_6$, it corresponds to side B8A6. The hinges can move independently crossing at one point. First, let's focus on the hinge part (shown in Figure 6(b)) which is enclosed in a square in the 3D model (shown in Figure 6(a)) using the analytical model of TMP created in Chapter 4. In Figure 6(b), the line segments A_1B_2 and B_8A_6 correspond to the 2 hinges described above, and the line segment A_1B_8 is the edge portion of bonding (a line segment that coincides when folded). As the triangle portion surrounded by the line segments A_1B_2, B_8A_6, and A_1B_8 serves as the portion of bonding, and the plane on which the line segments A_1B_2 and B_8A_6 overlap changes the angle while the change in the folded state, the adjacent parallelograms can move independently without deforming the surfaces. In flat folded state of Figure 5(b), the adjacent parallelograms partially overlap each other as shown, and in unfolded state of Figure 5(c), they move with contacting on one point as shown by point I.

On the other hand, Nojima Polyhedron also has been considered as rigid folding in [29], however it is not rigid folding as follows. Figure 7(a) shows one unit of NP's crease pattern. The portions painted in light blue become gluing parts. When folded, the line segment A_1B_2 coincides with the line segment A_6B_8. Here the movement of 2 adjacent trapezoidal surfaces with bonded parts between them is observed, by focusing on the trapezoids $A_1B_2B_3A_2$ and A_5B_7 B_8A_6. In NP, the surfaces of adjacent trapezoids are joined by one hinge (in trapezoid A_1B_2 B_3A_2, it corresponds to the side A_1B_2, while in trapezoid $A_5B_7B_8A_6$, it corresponds to the side B_6A_8, and they coincide with each other), and so the trapezoids move depending on the change of the folding states. Hence, it causes distortions, their surfaces are deformed.

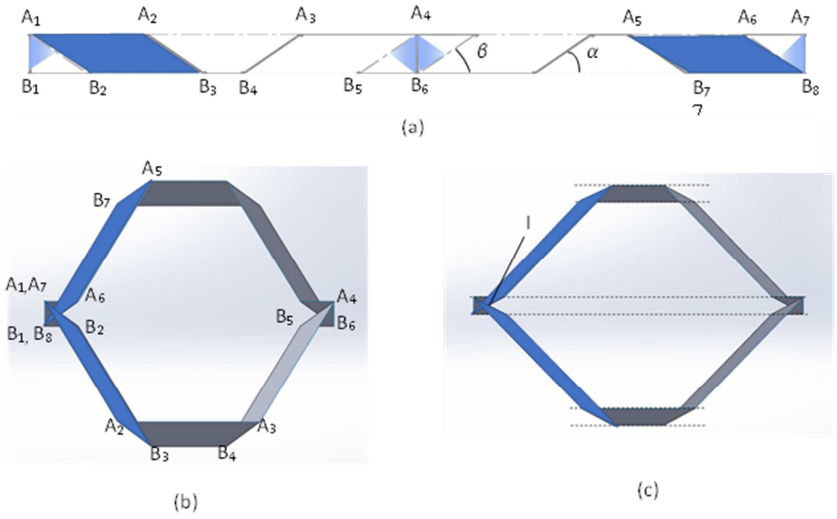

Figure 5. *TMP (a) 1 unit of patterns, (b) Top view of flat folded one, and (c) Top view of unfolded one.*

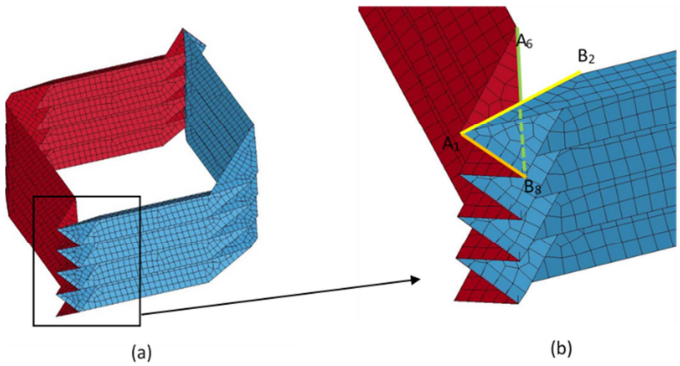

Figure 6. *TMP (a) 3D structure, and (b) Detail view of hinge parts.*

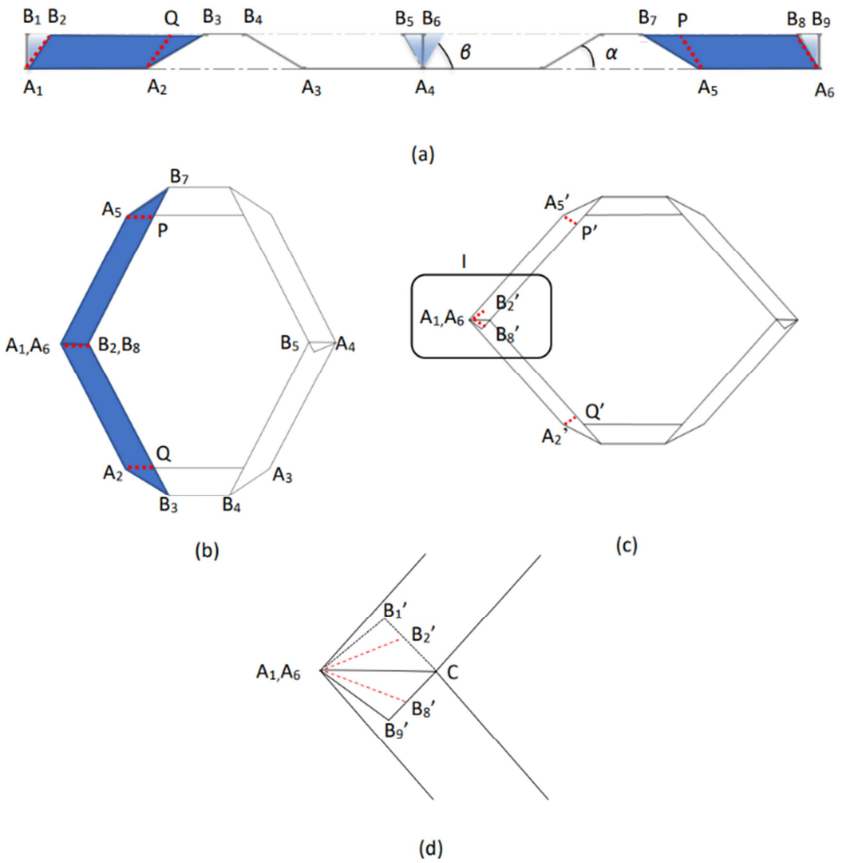

Figure 7. *NP (a) 1 unit of patterns, (b) Top view of flat folded one, (c) Top view of unfolded one, and (d) Detail view of a hinge part.*

Now, on the assumption that the position of the point A_1 (at the same position as the point A_6) does not move due to the change of the folding state, some line segments are focused on. When defining the point P such that $A_6B_8//A_5P$ on the line segment B_7B_8 and defining the point Q such that $A_1B_2//A_2Q$ on the line segment B_2B_3, in folded state of Figure 7(b), the line segment A_1B_2 coincides with the line segment A_6B_8, and the line segments A_5P, A_1B_2 (equals to the line segment A_6B_8) and A_2Q are parallel. In unfolded state of Figure 7(c), the line segment A_5P moves to the line segment A_5'P', and the line segment A_6B_8 parallel thereto moves to the line segment A_6B_8'. Likewise, the line segment A_2Q moves to the line segment A_2'Q', and the line segment A_1B_2 parallel thereto moves to the line segment A_1B_2'. Since the line segments A_5'P' and A_6B_8' are parallel and the line segments A_2'Q' and A_1B_2' are parallel, in the area surrounded by a rounded rectangle I, the line segments that coincide in folded state of Figure 7(b), do not coincide with each other in unfolded state of Figure 7(c). In Figure 7(d) enlarging the part surrounded by I in Figure 7(c), since adjacent trapezoids intersect with each other, it is impossible to move while keeping their shapes of surfaces. Therefore, as the mid-point between the points B_2' and B_8', a point C which is the intersection point of the straight lines obtained by extending the line segments B_1'B_2' and B_9'B_8' is taken. Then, the fact that when seen from above, both the points B_1' and B_9', and the points B_2' and B_8' are symmetrical with respect to the original line segment A_1B_2 (equals to the line segment A_6B_8) is used. With the assumption that the edges of the trapezoids are coincident at the point C, it is possible to create an analysis model in 3-dimension by using approximate coordinates, not by using exact coordinates.

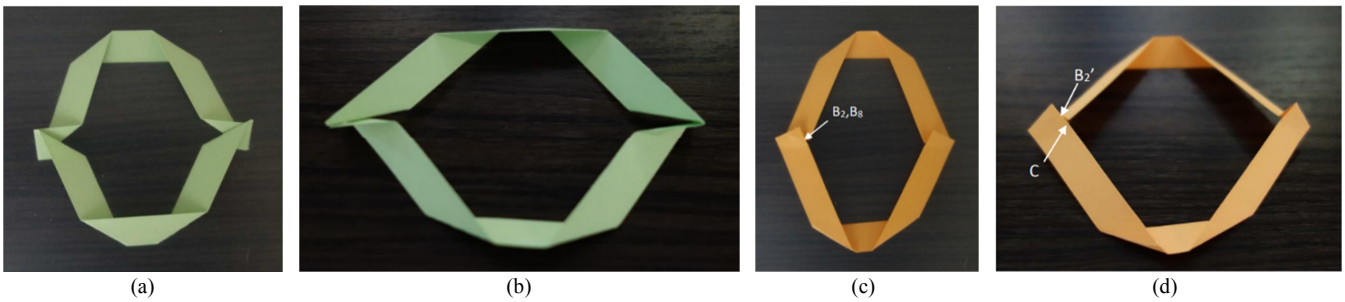

(a) (b) (c) (d)

Figure 8. *Paper model of TMP (a) 1 unit of flat folded one; (b) Unfolded one, and NP (c) 1 unit of flat folded one; (d) Unfolded one.*

Each example model of a rigid folding TMP and a non-rigid folding NP is represented by one paper unit. In the case of rigid folding TMP, without any deformation the folding is performed smoothly from flat folded to unfolded state as shown in Figure 8(a), (b) respectively. In the case of non-rigid folding NP, since some part deforms, the folding is not performed smoothly, so there are some reaction forces when unfolded. In Figure 8(c), the points B_2 and B_8 coincide with each other and become the edge point of the bonding. As shown in Figure 8(d), by setting a point C instead of the point B_2'(moved point B_2 when unfolded) as an edge point of the bonding, it is possible to make the 3-dimensioned model.

2.4. Discussion About Production Methods for NP and TMP

As far as the manufacturing method, the target model is not suitable because it is too complicated to manufacture as it is. It is conceivable that the flange parts and the main body parts are simplified to make the shape more easily manufacturable. As far as the flange parts, in the current shapes of NP/TMP, analytical models are created for the gluing surfaces of flange parts as they are. But in case of manufacturing, by omitting these parts, it is possible to reduce the material cost and the crushing force will be expected to be reduced. On the other hand, as far as the main body parts, the number of folding lines of the body parts is large in the current NP/TMP, and the both sections when viewed from the top look like a hexagon. If the cross-section shape is reduced by decreasing the number of folds, the both sections when viewed from the top look like a quadrilateral. It is expected that creating thus analytical model will have the effect of reducing the number of processes and reducing the crushing force. However, exploring them in detail here is omitted and it is left as a future issue.

Moreover, in consideration of its application to beverage cans, it is important to set the initial shape so that the deformation of the bottom shape due to the axial compression is slight.

Both TMP and NP can be folded in both axial and radial directions. As for TMP, there are already several reports, but the following things are not mentioned anywhere. For the discussion below, since both TMP and NP can be discussed similarly, only NP will be described in detail here. Once the bottom edge is constrained, it can be only folded in the axial direction. However, even if the lower end is fixed, the sections not directly restrained are spread to the radial direction under compression of axial direction. This behavior varies depending on the value of angle θ shown in Figure 9. For example, in the case of θ=0°, as it is compressed in the axial direction, it can be said that the distortion greatly spreads in the radial direction and the distortion on the upper end side by fixing the lower end becomes very large. On the other hand, when θ of the initial value is near to the angle of the largest one 150° to a certain extent, distortion becomes relatively small. For example, in the case of θ=145° shown in Figure 9(a) to θ=150°shown in Figure 9(b), the rate of change of θ is about 3%, which is applicable to an actual beverage can. It is important to take the change rate of the value of θ as small as possible when considering to do so, as it is done this time. Figure 10 shows the state of deformation by axial compression of NP and TMP for reference.

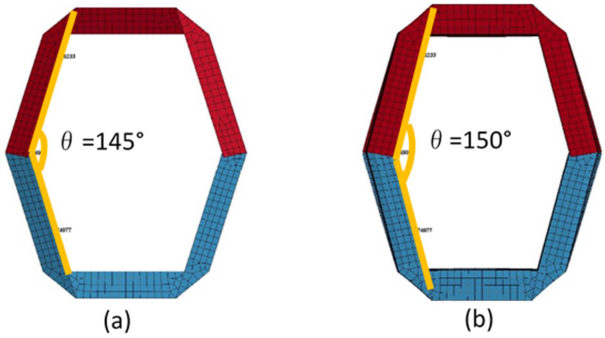

Figure 9. *Top shape (a) before crushing, (b) after crushing.*

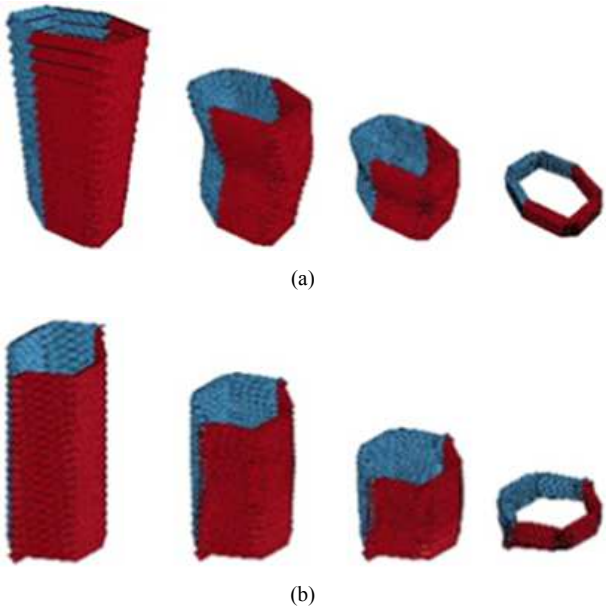

Figure 10. *Deformation under compression of axial direction (a) NP, (b) TMP.*

3. Parametric Expressions of Both Polyhedrons

3.1. Parametric Expression of Nojima Polyhedron

Figure 11 shows one unit pattern of NP. Figure 12 shows the slanted view of 3D NP unit cell. In Figure 11, the nodes (A_1, A_2, B_1, B_2, B_3) and (A_3, A_4, B_4, B_5, B_6) are symmetric with respect to the y-z plane. In Figure 12, the nodes (B_1, B_2, B_3, B_4, B_5, B_6) and (C_1, C_2, C_3, C_4, C_5, C_6) are symmetric with respect to the x-y plane. Therefore, by using 5 nodes (A_1, A_2, B_1, B_2, B_3), other nodes are automatically obtained. These 5 nodes are called as key nodes. The key nodes can be represented by 4 parameters (d, l, m, α) as follows. As shown in Figure 13, the lengths of each side and the angles of each corner in the development drawing are fixed values as follows.

$$|A_1A_2| = |A_3A_4| = m, |A_1B_1| = |A_4B_6| = d,$$
$$|A_2A_3| = l, \angle B_3A_2A_3 = \alpha, \angle B_2A_1A_2 = \beta = 2\alpha.$$

The lengths of each side are also constant as shown in Eq. (1).

$$|A_1B_2| = \frac{|A_1B_1|}{\sin(2\alpha)} = \frac{d}{\sin(2\alpha)}$$
$$|B_2B_3| = |A_1A_2| + \frac{d}{\sin(2\alpha)} = m + \frac{d}{\sin(2\alpha)}$$
$$|B_3B_4| = |A_2A_3| - \frac{2d}{\tan(\alpha)} = l - \frac{2d}{\tan(\alpha)} \quad (1)$$

Eq. (2) is obtained when the points A_1 and A_2 are expressed using varying δ according to the change in dihedral angle θ when the flat model is raised to a 3-dimensional shape.

$$A_1\begin{cases} x = \frac{|A_2A_3|}{2} + |A_1A_2|\cos(2\alpha - \delta) = \frac{l}{2} + m\cos(2\alpha - \delta) \\ y = 0 \\ z = 0 \end{cases}$$
$$A_2\begin{cases} x = \frac{|A_2A_3|}{2} = \frac{l}{2} \\ y = |A_1A_2|\sin(2\alpha - \delta) = m\sin(2\alpha - \delta) \\ z = 0 \end{cases} \quad (2)$$

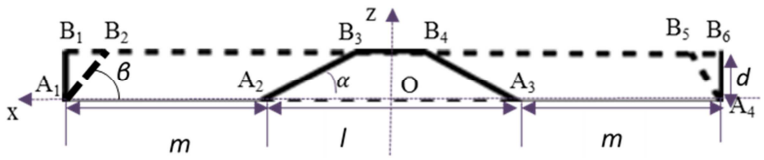

Figure 11. *One unit pattern of NP.*

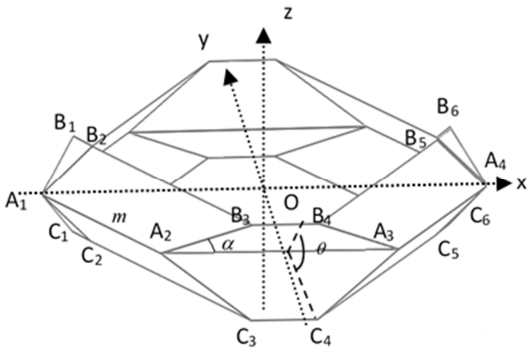

Figure 12. *The geometric characteristics of TMP (a)~(c).*

The points B_2 and B_3 are expressed in Eq. (3). From the points shown in Chapter 2, the coordinates are defined as follows;

$$B_2\begin{cases} x = \frac{|B_3B_4|}{2} + |B_2B_3|\cos(2\alpha - \delta) = \frac{l - \frac{2d}{\tan(\alpha)}}{2} + (m + \frac{d}{\sin(2\alpha)})\cos(2\alpha - \delta) \\ y = 0 \\ z = d\sin(\theta) \end{cases}$$
$$B_3\begin{cases} x = \frac{|B_3B_4|}{2} = \frac{l - \frac{2d}{\tan(\alpha)}}{2} \\ y = |B_2B_3|\sin(2\alpha - \delta) = (m + \frac{d}{\sin(2\alpha)})\sin(2\alpha - \delta) \\ z = d\sin(\theta) \end{cases} \quad (3)$$

Here, y coordinate of the point B_2 is always 0, and the length $|B_2B_3|$ is constant.
The point B_1 is on the same straight line as the line segment B_2B_3, and so the coordinates are determined as shown in Eq. (4).

$$K = \frac{|B_1B_2|+|B_2B_3|}{|B_2B_3|}$$

$$\overrightarrow{B_3B_1} = K\overrightarrow{B_3B_2}$$

$$B_1\begin{cases} x = K(x_{B2} - x_{B3}) + x_{B3} \\ y = K(y_{B2} - y_{B3}) + y_{B3} \\ z = d\sin(\theta) \end{cases} \quad (4)$$

The length $|A_1B_2|$ is obtained from Eqs. (2) and (3). Since this value is equal to the value of Eq. (1), Eq. (5) can be obtained. This is the equation held between the 3 angles α, δ and θ.

$$\cos(2\alpha - \delta) = 2\cos^2(\alpha) - \sqrt{1 - (\sin(\theta)\sin(2\alpha))^2} \quad (5)$$

The coordinates are determined by approximation from the reason why the solid model with the accurate coordinates is not formed because the surfaces are deformed while folding, since NP is not rigid folding. As a result, in the trapezoid $A_1A_2B_3B_2$ shown in Figure 13, the length $|A_2B_3|$ should be originally constant, but depending on the dihedral angle θ, the length changes from the exact one. The length $|A_2B_3|$ is different on condition of θ=0 ° or 90 °, and on condition of 0°<θ<90°, and so 2 equations as follows are obtained.

When θ=0° or 90°, Eq. (6) is obtained by referring to Figure 13.

$$|A_2B_3|_{\theta=0°,90°} = \sqrt{\left\{\frac{d}{\tan(\alpha)}\right\}^2 + d^2} \quad (6)$$

When 0°<θ<90°, the distance between the points A_2 and B_3 is given by Eq. (7) from the parameters of each coordinate.

$$|A_2B_3|_{0<\theta<90°} = \sqrt{\left\{\frac{d}{\tan(\alpha)}\right\}^2 + \left\{\frac{\sin(2\alpha-\delta)}{\sin(2\alpha)}d\right\}^2 + \{d\sin(\theta)\}^2} \quad (7)$$

Relationship between the dihedral angle θ and the length $|A_2B_3|$, when α=30 ° and d=1mm, is shown in Figure 14. Around θ=50°, the error of the length $|A_2B_3|$ from Eq. (7) becomes maximum. The above is confirmed by substituting numerical values into the equation. According to Eq. (5)

$$\sin^2(2\alpha - \delta) = 1 - \{2\cos(\alpha) - \sqrt{1 - \{\sin(\theta)\sin(2\alpha)\}^2}\}^2$$

By substituting this into Eq. (7)

$$|A_2B_3|_{0<\theta<90°}{}^2 = f(\theta) = 2\sin^2\theta + 4\sqrt{1 - \frac{3}{4}\sin^2\theta}$$

When calculating the maximum value of f(θ), it is when sin θ $=\sqrt{\frac{7}{12}}$, i.e. θ = 49.79703411, and the maximum value of f(θ) is $\frac{25}{6}$.

This results in max $|A_2B_3|_{0<\theta<90°}=\sqrt{f(\frac{25}{6})}$ = 2.041241452.

By Eq. (6), $|A_2B_3|_{\theta=0°,90°}$ = 2, and so the length $|A_2B_3|$ is increased about 2.1% at maximum.

As described above, since the coordinates of some points cannot be indicated accurately by the parameters in the case of NP, they are obtained by approximation. The length $|A_2B_3|$, which is one side of the trapezoids $A_1A_2B_3B_2$ and $A_2A_3B_4B_3$, may change depending on the dihedral angle θ. However, the value of its length is about 2% of all values at most, so it is within the allowable error for this FEM simulation.

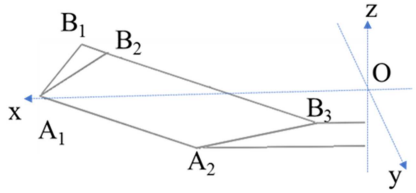

Figure 13. *The geometric characteristics of TMP (a)~(c).*

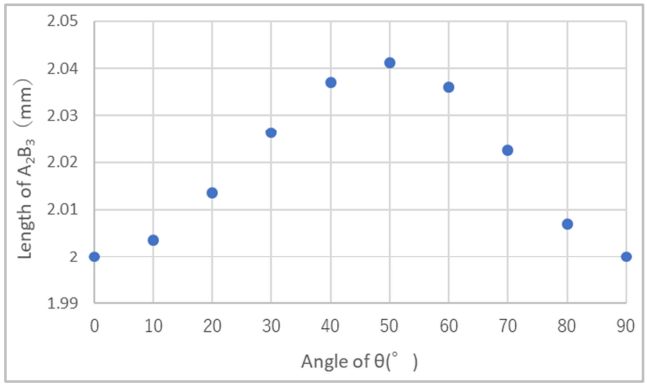

Figure 14. *The geometric characteristics of TMP (a)~(c).*

3.2. Parametric Expression of Tachi – Miura Polyhedron

As the same as NP, the key nodes of TMP shown in Figure 15 are expressed by 4 parameters (d, l, m, α) as follows.

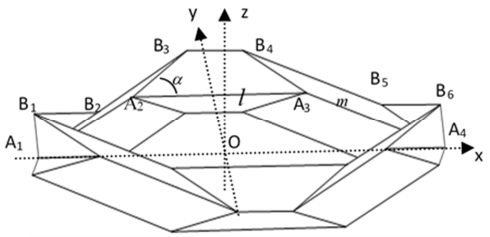

Figure 15. *Slanted view of 3D TMP unit cell. The key-nodes of the unit cell and the glide symmetry structural relationship are represented.*

$$|B_2B_3| = m$$

$$|B_3B_4| = |A_2A_3| - \frac{2d}{\tan(\alpha)} = l - \frac{2d}{\tan(\alpha)}$$

$$|A_1A''| = |A''B''| = \frac{|A_1B_1|}{2\sin(2\alpha)} = \frac{d}{2\sin(2\alpha)}$$

$$A_1\begin{cases} x = \frac{|A_2A_3|}{2} + |A_1A_2|\cos(2\alpha - \delta) = \frac{l}{2} + m\cos(2\alpha - \delta) \\ y = \frac{|A_1B_1|}{2}\cos(\theta) = -\frac{d}{2}\cos(\theta) \\ z = 0 \end{cases}$$

$$A_2\begin{cases} x = \frac{|A_2A_3|}{2} = \frac{l}{2} \\ y = \frac{|A_1A_2| - |A_1A''|}{2}\cos(\theta) = -\frac{d}{2}\cos(\theta) \\ z = 0 \end{cases}$$

$$B_1\begin{cases} x = x_A = \frac{l}{2} + m\cos(2\alpha - \delta) \\ y = -y_A = \frac{d}{2}\cos(\theta) \\ z = d\sin(\theta) \end{cases}$$

$$B_2\begin{cases} x = \frac{|B_3B_4|}{2} + |B_2B_3|\cos(2\alpha - \delta) = \frac{l - \frac{2d}{\tan(\alpha)}}{2} + m\cos(2\alpha - \delta) \\ y = y_B = \frac{d}{2}\cos(\theta) \\ z = d\sin(\theta) \end{cases}$$

$$B_3\begin{cases} x = \frac{|B_3B_4|}{2} = \frac{l - \frac{2d}{\tan(\alpha)}}{2} \\ y = (|B_2B_3| + |A''B''|)\sin(2\alpha - \delta) = (m + \frac{d}{2\sin(2\alpha)})\sin(2\alpha - \delta) \\ z = d\sin(\theta) \end{cases}$$

Eq. (8) obtained from the difference between the y coordinates of the points A2 and B3 is an equation held between the 3 angles α, δ and θ.

$$y_A = y_B, -d\cos(\theta) \Rightarrow \sin(2\alpha - \delta) = \cos(\theta)\sin(2\alpha) \tag{8}$$

In the case of TMP, the length$|A_2B_3|$ is obtained as in the case of NP. When θ=0°or 90°, Eq. (9) is obtained by referring to Figure 16.

$$|A_2B_3|_{\Theta=0°,90°} = \sqrt{\left\{\frac{d}{\tan(\alpha)}\right\}^2 + d^2} \tag{9}$$

When 0°<θ<90°, the distance between the points A_2 and B_3 is given by Eq. (10).

$$|A_2B_3|_{0<\theta<90°} = \sqrt{\left\{\frac{d}{\tan(\alpha)}\right\}^2 + \left\{\frac{\sin(2\alpha-\delta)}{\sin(2\alpha)}d\right\}^2 + \{d\sin(\theta)\}^2} \tag{10}$$

When substituting Eq. (8) into Eq. (10) results in Eq. (9), the length $|A_2B_3|$ is constant and so it does not depend on θ.

$$|A_1B_1| = d,\ |A_1B_2| = \sqrt{\left\{\frac{d}{\tan(\alpha)}\right\}^2 + d^2},\ |B_1B_2| = \frac{d}{\tan(\alpha)}$$

Here, in the case of TMP, the length of each side of the shape, that is, the length of each side of triangle $A_1B_1B_2$, parallelogram $A_1A_2B_3B_2$ or trapezoid $A_2A_3B_4B_3$ does not depend on θ. Since d, l, m and α are constant, the length of each side of the triangle $A_1B_1B_2$ is as follows and does not depend on θ. Figure 16 shows one unit pattern of TMP.

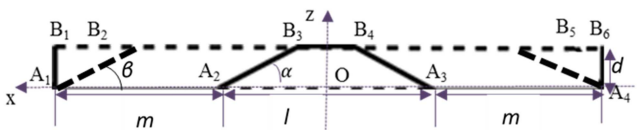

Figure 16. *One unit pattern of TMP.*

Similarly, the length of each side of the parallelogram $A_1A_2B_3B_2$ is as follows and does not depend on θ.

$$|A_2B_3| = |A_1B_2| = \sqrt{\left\{\frac{d}{\tan(\alpha)}\right\}^2 + d^2}$$

$$|A_1A_2| = |B_2B_3| = m$$

Equivalently, the length of each side of the trapezoid $A_2A_3B_4B_3$ is as follows due to the symmetry, not dependent on θ.

$$|A_2A_3| = l \; |A_2B_3| = |A_3B_4| = \sqrt{\left\{\frac{d}{\tan(\alpha)}\right\}^2 + d^2}$$

$$|B_3B_4| = l - \frac{2d}{\tan(\alpha)}$$

From the above, no deformation occurs on the each surface. In this way, in the case of TMP, it can be said that the coordinates of each point can be accurately represented by parameters.

4. Availability for Folding Aluminum Cans of NP and TMP

4.1. Analysis Model and Method

Figure 17 shows the analysis model generated using LS-Pre-Post. The finite element system used is LS-DYNA [34] and the model has around 20000 nodes and 20000 quadrilateral reduced integration Belytschko-Tsay shell elements [35]. The penalty contact condition is defined between the structure and the rigid wall and also defined for structure itself with the coefficient of friction is 0.1. For the material, aluminum which has the characteristics of Table 3 is used. As the load condition, the initial velocity of 2000 mm/s is given to the rigid wall, and the structure is compressed. And the boundary condition is that the bottom nodes of the structure are fixed completely. Crushing analysis of pairing origami structure is carried out in the time direction explicit method in finite element method. Although problem here is originally a static problem, it is a strong nonlinear problem including contact and large deformation, and so it does not easily converge by static analysis [36]. Therefore, it is executed as quasi-static analysis.

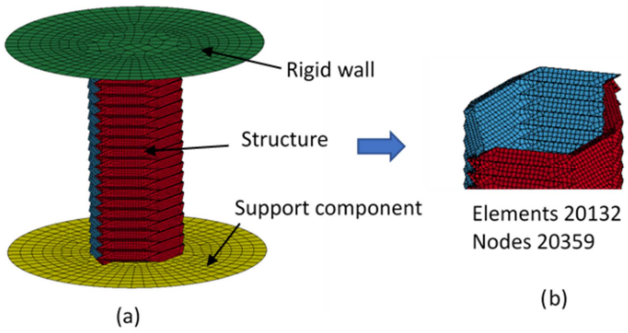

Figure 17. *(a) The analysis model (b) Few steps of the model.*

Table 3. *Material properties of the structure.*

Young's modulus	70 GPa
Poisson's ratio	0.33
Density	2.7×10^{-6} kg/mm^3
Yield stress	100 MPa
Tangent modulus	280Mpa
Thickness	0.1mm

4.2. Optimization Analysis

The target problem is to minimize the maximum crushing force of each pairing structure by using 3 design variables of (l, α, θ) between the points as follows. The load displacement diagram for optimal models is shown in Figure 18. As shown in Figure 18, at first the load value rises, and next remains almost unchanged, and then the load rises again and at last reaches a status, where the load rises high and the deformation hardly changes due to its bulkiness. In the automobile company, it is referred to as "bottoming phenomenon" and its last is called "deformation stop line". The target problem is between the points A and B. The point A is the point after the load value rises at first, and the point B is the point just before the load rises again. For the optimization, the design of experiments method L9 which is one of the response surface optimization methods is used. The conditions of the optimization analysis are shown as below.

(a) Design variables

l [40, 60]; The length of one side of the horizontal cross section. α [30, 40]; The base angle of the trapezoid whose base side length is "l". θ [30, 50]; The dihedral angle.

(b) Constraints

Weight less than the standard commercially available cans of aluminum. The standard weights are about 15g per a 350 ml can and about 20g per a 500ml can, so the weight is set lighter than 40g by proportional calculation because there is a request for bigger capacity which is from 1000 ml to 1500 ml. The design variables l [40, 60] above is set by this constraint.

(c) Objective function

To minimize the maximum crushing force. As for the ranges of the design variables, they are set so that the horizontal cross section shape is as close to a circle shape as possible.

The flowchart of the optimization is shown in Figure 19. The 9 data sets shown in Table 4 are used for the sample data. After solving by LS-DYNA, the solution is obtained by optimization software LS-OPT.

The design variables (l, α, θ) and the results (crushing force, weight) are summarized and calculation of optimization by the response surface optimization method are performed, but at least 10 sampling points are necessary to create the second order response surface. It becomes the response surface of the primary order in Figure 20. As a result, all optimum solutions are obtained at boundary values. After analyzing with LS-DYNA, the optimal design variables (l, α, θ) and the results (maximum crushing force) are obtained. All the results including volumes and weights are shown in Table 5.

l is the maximum value of 60 mm in both NP and TMP, and α is the maximum value of 40 ° in NP, and the intermediate value of 35 ° in TMP. It is considered that the combinations of the parameters make the maximum cross

section area with respect to the circumferential length respectively. θ is 30° of the minimum value in both NP and TMP, seems to be due to the fact that the smaller the dihedral angle is, the less the crushing force is required for crushing.

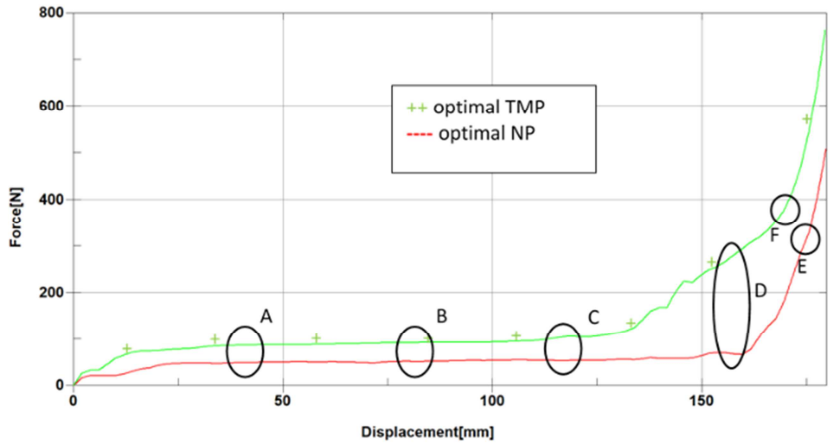

Figure 18. *Relationship between Displacement and Force. The curve with + shows optimal TMP, and another curve shows optimal NP.*

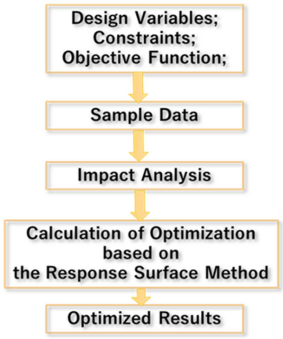

Figure 19. *Flow chart of optimization.*

Table 4. *L9 analysis table.*

No.	l(mm)	α(°)	θ(°)
1	40	30	30
2	40	35	40
3	40	40	50
4	50	30	40
5	50	35	50
6	50	40	30
7	60	30	50°
8	60	35	30
9	60	40	40

Table 5. *Optimal dimensions, volume, weight and maximum crushing force.*

	Optimal NP	Optimal TMP
l[mm]	60	60
α[°]	40	35
θ[°]	30	30
Volume[ml]	1242.5	1293.3
Weight[g]	32.8	29.0
Maximum crushing force[N]	51.9	89.8

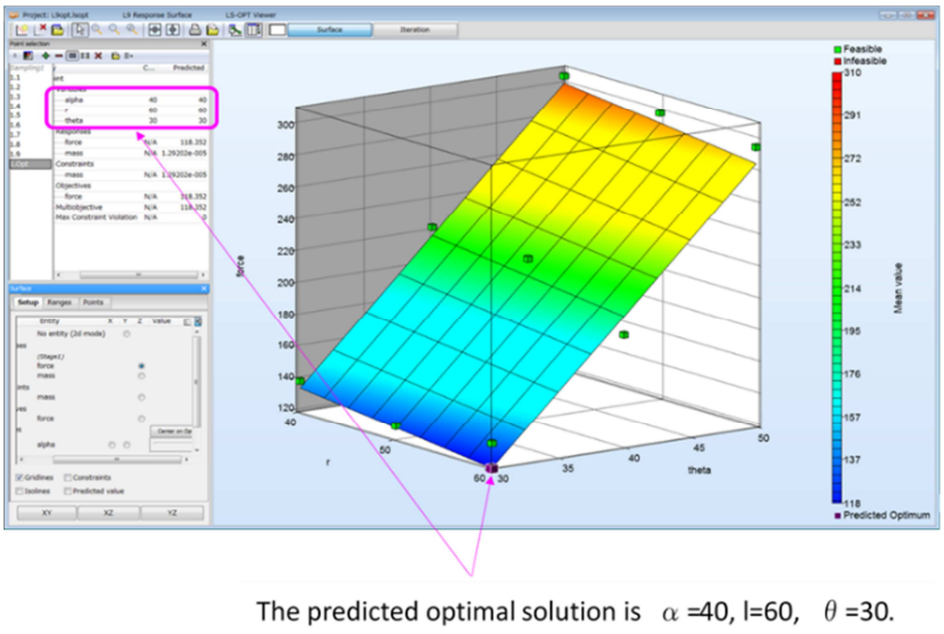

Figure 20. *Result of optimization analysis.*

The weight is 32.8g in NP and 29.0g in TMP, both of which are less than the constraints and are reasonable. The volume is also 1242.5ml in NP and 1293.3ml in TMP, both of which are within the constraints and are reasonable.

In Figure 18, it seems that the displacement in NP of the range from 20 to 150 mm and that in TMP of the range from 20 to 120 mm are the states mentioned above as between the points A and B.

According to the study by Kamata et al. [26], the average value of the force applied by a man when holding the can with one hand and compressing it in the axial direction with the other hand is about 160N. The results of maximum crushing force are 51.9N in NP, 89.8 N in TMP. Both are less than 160N, and so they are reasonably crushed.

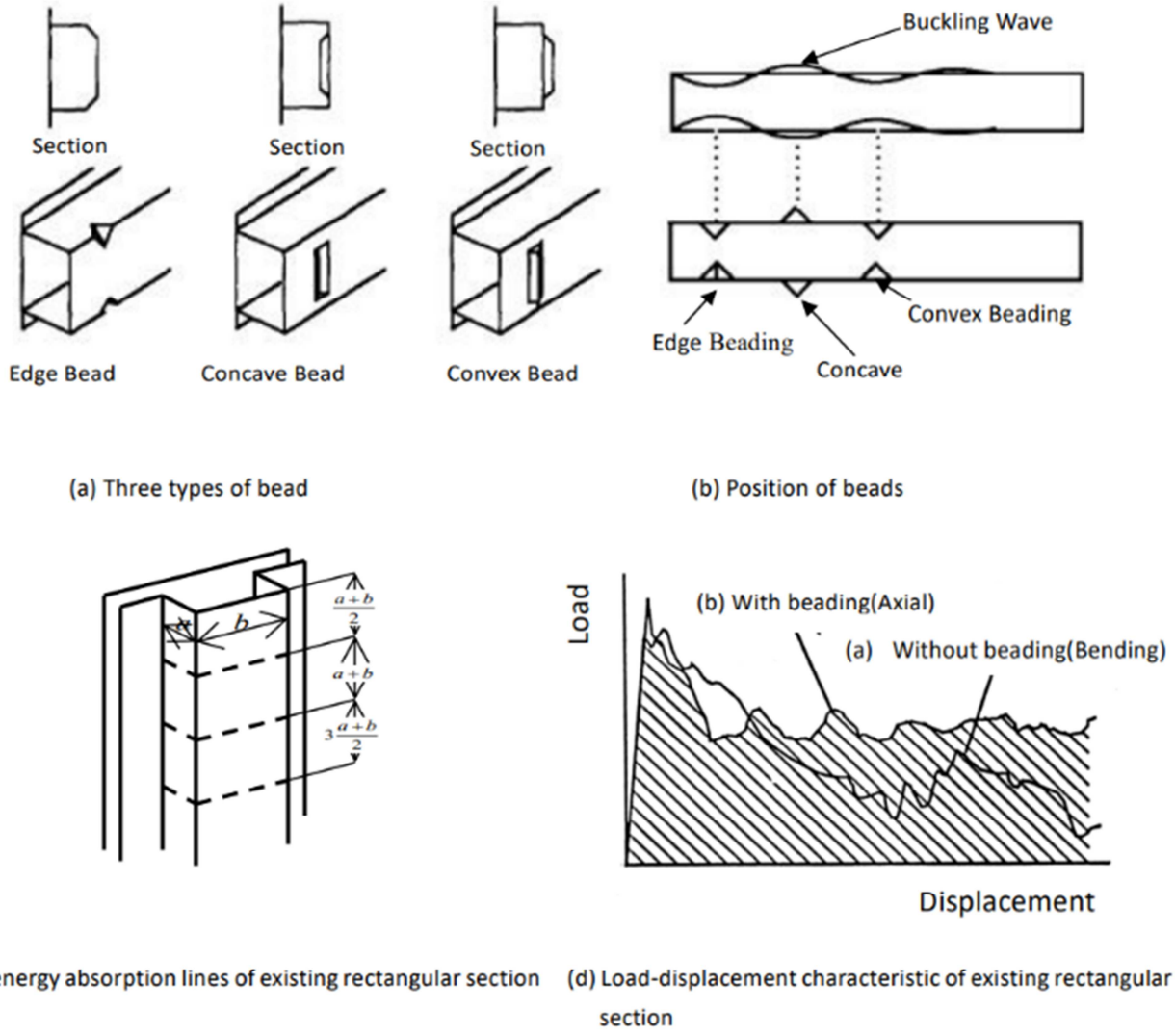

Figure 21. *The position of beads can control the buckling wave form. There are three types of beads shown in (a). Edge bead means cutting a corner of the section (edge of the member); concave bead means projection toward the inside of the member; convex bead means projection toward the outside of member. The most effective bead arrangement is illustrated in (b). Concave beads, convex beads, a couple of edge beads should be placed on the concave parts, on the convex parts, the first concave part of the buckling wave respectively. Ideal axial crush is obtained when the crush happens at the interval of from the upper side of the existing rectangular section as shown in (c). As shown in (d), when the bending in the existing rectangular section occurs, the reaction force will not transmit downward and the amount of energy absorption.*

Here, in the energy absorbing material of the hollow cross section used in existing automobile vehicles, the reaction force immediately decreases as the bending occurs, but the reaction force itself does not change in both case of NP and TMP. Compared with the rectangular cross-section hollow structure of Figure 21 which simulates the energy absorbing material used in the current vehicle, there is a difference as follows. As shown in Figure 21(c), where crushing occurs is at the interval of (a+b)/2 from the upper end. If the collapse occurs at this interval, the crush propagates to the lower end with the same period length, but if collapse begins to occur at a position deviated from this interval, it becomes bent from there, and the reaction force does not propagate to the lower end. Hagiwara et al., showed that members can be induced to

accordion-like crush by arranging corner beads and concave / convex beads as shown in Figure 21(a) according to buckling mode [37-39]. For this reason, the bead shown in Figure 21(a) is provided in the energy absorbing material of the current vehicle. On the other hand, in both NP and TMP, the interval between the collapsed lines is shorter than the current energy absorbing material by 0.2 times. As a result, as shown in Figure 21(d), the load displacement characteristic of the energy absorbing material of the current vehicle is (a+b)/2, and there is periodicity of length of buckling half wavelength, whereas no periodicity is observed in NP and TMP, and even when one collapsed line becomes a fold line, it is shown that reaction force tends to propagate downward.

In the case of NP, the load value begins to rise near 150 mm in Figure 18(D), and when it exceeds 175 mm in Figure 18(E), it also increases sharply. In the case of TMP, the load value begins to rise near 120 mm in Figure 18(C), and it increases sharply when it exceeds 170 mm in Figure 18(F). This is called a state of "deformation stop line", and it seems that such a state will be obtained when the displacement reaches about 90% of its original length.

The load value of TMP is higher than that of NP overall, and TMP reaches bottoming phenomenon with a shorter displacement than NP. Here, the reason is considered.

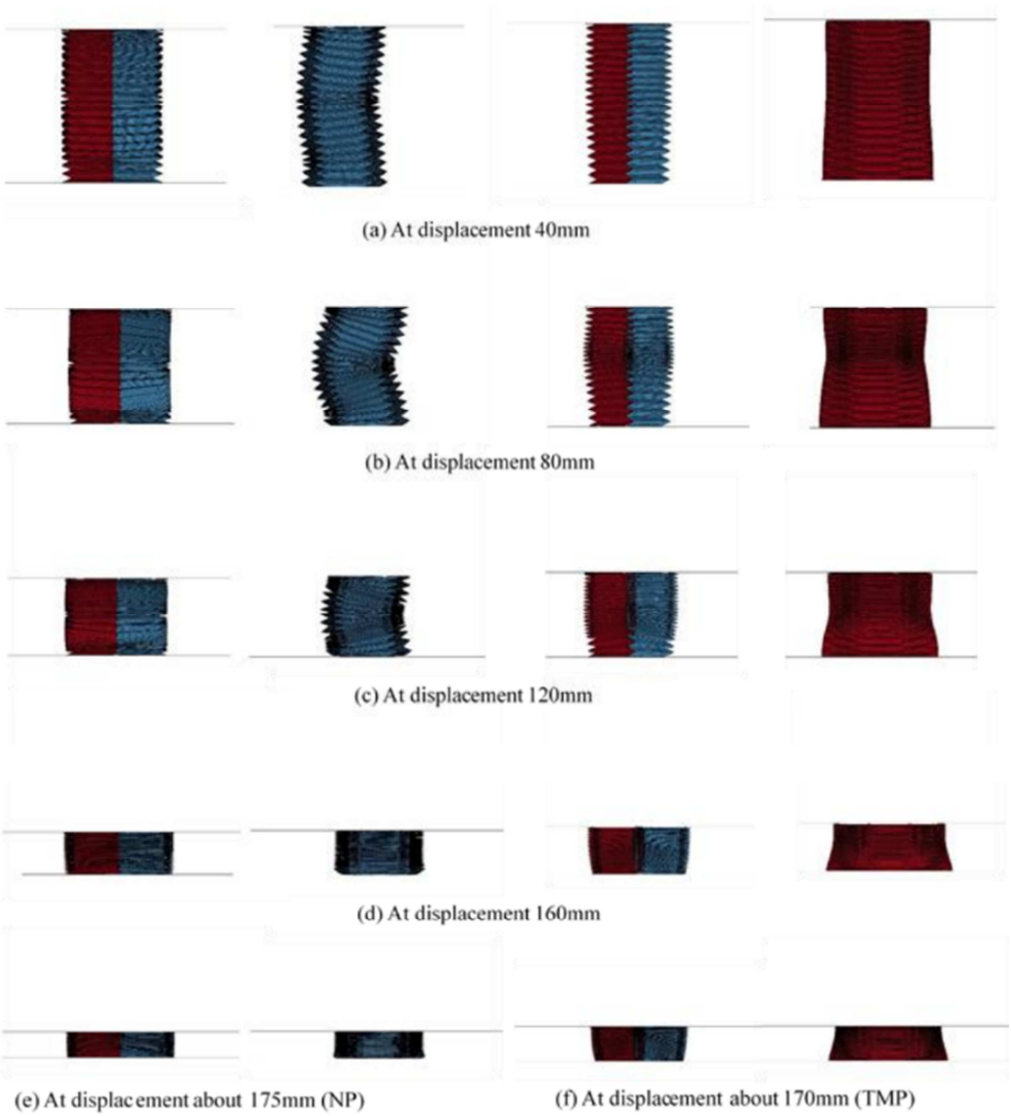

Figure 22. *Crush deformations of each pairing structure at different displacement; 2 rows from the left show NP (Front view on the left, and right-side view on the right) and 2 rows from the right show TMP (Front view on the left, and left-side view on the right).*

For the deformation of NP and TMP in Figure 22, the displacements ranging from 40 to 160 mm are shown as from (a) to (d) every 40 mm. (e) and (f) are diagrams showing the deformation in the vicinity where the bottoming phenomenon of NP and TMP starts (at the displacement of 175mm in NP, and 170mm in TMP). (a) to (f) in Figure 22 correspond to from A to F in Figure 18, respectively.

In the NP model on the left side of Figure 22, viewed from the front (the left one of two illustrations), it seems to be folded straight. However, viewed from the right side (the right one of two illustrations), it starts to deform so that the central portion of the height bends laterally when the

displacement shown in Figure 22(a) reaches nearly 40mm. It bends most horizontally when the displacement shown in Figure 22(b) reaches nearly 80mm. As the compression progresses, the bending goes straight back and it becomes straight completely when the displacement shown in Figure 22(d) reaches nearly 160mm. It folds almost straight in the end. Looking at the bending part at this time, deformation that bends at the hinge part of pairing origami structure has occurred, and there is no deformation that bends at the other main body parts. This is because NP is not rigid folding. The distortion is concentrated particularly on the weakest hinge part of the structure.

In the TMP model on the right side of Figure 22, viewed from the front (the left one of two illustrations), it is folded straightly while deforming into a shape in which the width of the central part swells when the displacement shown in Figure 22(a) reaches nearly 40mm. On the other hand, viewed from the left side (the right one of two illustrations), the transverse width of the central part is deformed to a concave shape when the displacement shown in Figure 22(b) reaches nearly 80mmIn the end, it is folded straightly. It seems that TMP is folded relatively straightly without deforming like NP having some distortion in the hinge part, because it is a rigid folding.

Also, in the case of NP, when comparing figures viewed from the right side, the lowermost wall rises upward on Figure 22(d), whereas it downs on Figure 22(e). On the other hand, in the case of TMP, comparing the figure viewed from the left side, the lower half of the model has a rounded shape as shown in Figure 22(c). As the displacement approaches from (d) to (f) in Figure 22, it becomes a trapezoidal shape which linearly spreads downward.

It is supposed that both NP and TMP have some difficulty in folding due to complete fixing of the bottom surface, and this is thought to be greater influence in case of TMP than of NP. Figure 23 shows a view of both models from the bottom at the end of compression. Compared with NP, TMP has larger crushed portion and protrudes from the wall of the bottom surface (the dark displayed parts). Therefore, to compare NP and TMP, by using the formula of Chapter 3, we calculate the length and width of the bottom surface before and after crushing, respectively and observe the changes. Table 6. shows the changes in length and width of the bottom surfaces before and after crushing with NP and TMP. Rate of change is a numerical value which normalized the length after crushing with the length before crushing. In NP, the length changes little in the vertical direction and decreases by 10% in the horizontal direction, otherwise in TMP the length increases by 20% in the vertical direction and decreases by 20% in the horizontal direction. This is also considered as the cause of the load value becoming higher as a whole in TMP compared with NP.

Figure 23. *Bottom view of each pairing structure after crushing. Left side is NP and right side is TMP.*

Table 6. *Comparison of change rate in vertical and horizontal length between NP and TMP.*

NP	Before crushing	After crushing	Rate of change
Vertical length	105.1	108.6	1.0
Horizontal length	87.3	75.6	0.9

TMP	Before crushing	After crushing	Rate of change
Vertical length	90.6	104.6	1.2
Horizontal length	112.3	90.8	0.8

5. Summary

Results are as follows.

1. 2 kinds of pairing origami structures for foldable cans, NP and TMP are investigated for the first time. They can be manufactured cheaply by accordion type folding and showed the possibility for practical use. Both TMP and NP are promising because folding up to about 70% in TMP, 80% in NP of its original length is possible with a force of 160 N or less which is an equivalent force of human hands.
2. "A rigid folding or not" is a popular interest in the world of origami engineering, however, it is difficult to distinguish it. Here, the rigid foldability of both NP and TMP by an easy method of examining the figure geometrically and by a quantitative analysis focused on the length of each side, are investigated and it is shown that TMP is a rigid folding, and by contrast, NP is not a rigid folding.
3. It is demonstrated that the rigid folding has an advantage to represent always the structural shape with design variable parametrically even though the structural shape changes at each step in an optimization routine. NP, which is not a rigid folding, could express the structural shape approximately the same way with TMP, however, its credibility is needed to be confirmed. As the result of examination with NP this time, it is found that the maximum error is 2%, which is within the allowable range.
4. An analysis on an optimized model which minimizes the maximum crushing force is carried out. Then it is found that No-rigid-folding NP had deformations at the hinge parts, but Rigid-folding TMP had none. In both

cases, the main body portion is folded until the end. In other words, whether a rigid folding or not has some influence on its deformation mode, but it is shown that it has no influence on the purpose to investigate its possibility for industrialization.

5. This is the first step to make sure that the pairing origami structure is effective as foldable can. Although it is possible to fold, it is concerned that the strength in the radial direction maybe weak and the shape may not be always easy to hold. As our future work, it is necessary to check the strength in the radial direction and consider the comfortableness when it is held and folded.

Acknowledgements

This work is supported by the MIMS Joint Research Project (FY2021). The authors appreciate Mathematical Sciences, Meiji Institute for Advanced Study of Mathematical Science for kind support and cooperation.

References

[1] Tokura, S., & Hagiwara, I. (2010). Forming Process Simulation of Truss Core Panel, Journal of Computational Science and Technology, 4 (1), 25-35 (Release Date: March 30, 2010).

[2] Tokura, S., & Hagiwara, I. (2010). A Study for the Influence of Work Hardening on Bending Stiffness of Truss Core Panel, J. Appl. Mech., 77/031010-1-031010-6(2010-5).

[3] Tokura, S., & Hagiwara, I. (2011). Shape Optimization to Improve Impact Energy Absorption Ability of Truss Core Panel, Journal of Computational Science and Technology, 5 (1), 1-12, (2011-1).

[4] Hedgepeth, J. M. (1989). Structures for remotely deployable precision antenna, NASA Contract Report, 182065.

[5] Guest, S. D., & Pellegrino, S. (1992). In extensional wrapping of flat membranes, First International Conference on Structural Morphology, Montpellier, R. Motro and T. Wester, eds., 203-215.

[6] Sogame, A., & Furuya, H. (2000). Conceptual study on cylindrical deployable space structures, Deployable Structures: Theory and Applications, S. Pellegrino and S. D. Guest (Eds.), Kluwer Academic Publishers, SMIA 80, 383-392.

[7] Shirasawa, Y., Mori, O., & Miyazaki, Y. (2012). Evaluation of membrane dynamics of IKAROS based on flight result and simulation using multi-particle model, Transactions of the Japan Society for Aeronautical and Space Sciences 10 (ists28) Po_4_21 - Po_4_26.

[8] Morgan, J., Magleby, S. P., & Howell, L. L. (2016). An approach to designing origami-adapted aerospace mechanisms, Journal of Mechanical Design, 138 (5). doi: 10.1115/1.4032973.

[9] W, S., Ze, Q., Dai, J., Udipi, N., Paulino, G. H., & Zhao, R. (2021). Stretchable origami robotic arm with omnidirectional bending and twisting, PNAS, 118, 2110023118.

[10] Hanna, B. H., Lund, J. M., Lang, R. J., Magleby, S. P., & Howell, L. L. (2014), Waterbomb base: a symmetric single-vertex bistable origami mechanism, Smart Materials and Structures, 23, 094009.

[11] Yasuda, H., Tachi, T., Lee, M., & Yang, J. (2017), Origami-based tunable truss structures for non-volatile mechanical memory operations, Nature Communications, 8, 962.

[12] Xiang, X. M., Lu, G., & You, Z. (2020), Review /Energy absorption of origami inspired structures and materials, Thin-Walled Structures, 157, December 2020, 107130.

[13] Song, J., Chen, Y., & Lu, G. (2012), Axial crushing of thin-walled structures with origami patterns. Thin-Walled Structures, 54: 65-71.

[14] Ma, J., & You, Z. (2013), Energy absorption of thin-walled square tubes with a pre-folded origami pattern-part i: geometry and numerical simulation, Journal of Applied Mechanics, 81: 011003--11.

[15] Garrett, D., You, Z., & Gattas, J. M. (2016), Curved crease tube structures as an energy absorbing crash box, ASME 2016 International Design Engineering Technical Conferences and Computers and Information in Engineering Conference, Charlotte, North Carolina.

[16] Ma, J., Hou, D., Chen, Y., & You, Z. (2016), Quasi-static axial crushing of thin-walled tubes with a kite-shape rigid origami pattern, Numerical simulation, Thin-Walled Structures. 100: 38-47.

[17] Wang, B., & Zhou, C. (2017), The imperfection-sensitivity of origami crash boxes. International Journal of Mechanical Sciences, 121: 58-66.

[18] Zhou, C., Zhou, Y., Wang, B. (2017), Crashworthiness design for trapezoid origami crash boxes. Thin-Walled Structures, 117, 257-67.

[19] Yang, K., Xu, S., Shen J, Zhou, S., & Xie, Y. M. (2016), Energy absorption of thin-walled tubes with pre-folded origami patterns Numerical simulation and experimental verification, Thin-Walled Structures, 103, 33-44.

[20] Yang, K., Xu, S., Zhou, S., & Xie, Y. M. (2018), Multi objective optimization of multi-cell tubes with origami patterns for energy absorption, Thin-Walled Structures, 123, 100-13.

[21] Hagiwara, I. & Nadayosi, S. (2003), Folding Process of Cylindrical Structures Using Origami Model, International Journal of Automotive Engineering, 34 (4), 145-149 (in Japanese).

[22] Hagiwara, I., Yamamoto, C., Tao, X. & Nojima, T. (2004), Optimization for crush characteristics of cylindrical origami structure using reversed spiral model, Transactions of the Japan Society of Mechanical Engineers, Series A, 70 (689), 36-42 (in Japanese).

[23] Wu, Z., Hagiwara, I., & Tao, X. (2007), Optimization of crush characteristics of the cylindrical origami structure, Int. J. Vehicle Design, 43 (1-4), 66-81.

[24] Zhao, X., Kong, C., Yang, Y., and Hagiwara, I. (2021), Reversed torsion-type crush energy absorption structure and its inexpensive partial-heating torsion manufacturing method based on origami engineering, Journal of Manufacturing Science and Engineering. doi: 10.1115/1.4052438.

[25] Nojima, T. (2000), Modelling of folding patterns in flat membranes and cylinders by using origami, Transactions of the Japan Society of Mechanical Engineers, Series C, 66 (643), 1050-1056 (in Japanese).

[26] Kamata, Y., Itoh, K., Kawamura, T., Honda, T., Matsugi, Y., & Ishimura, T. (2012), Development of easily folded up PET bottle, Transactions of the Japan Society of Mechanical Engineers, Series C, 78 (789), 456-466 (in Japanese).

[27] Ario, I. (2011), Cylindrical container and its manufacturing method, Patent number 4769976 (in Japanese).

[28] Hagiwara, I., Nara, C., & Yang, Y. (2022), Development of new foldable polyethylene terephthalate bottles, Journal of Advanced Simulation in Science and Engineering (JASSE), 9 (2), 158-177.

[29] Sugiyama, F. (2016), Pairing origami for manufacturing, Journal of Japan Society of Mechanical Engineers, 119 (1175), 14-15 (in Japanese).

[30] Nojima, T. (2015), 3D Origami for Monozukuri Proposal of Pairing Origami, Nippon Origami Association. ISBN: 978-4-86540-040-3 (in Japanese).

[31] Miura, K., & Tachi, T. (2010), Synthesis of rigid-foldable cylindrical polyhedral, Journal of the International Society for the Interdisciplinary Study of Symmetry, Symmetry: Art and Science, 204-213.

[32] Yang, Y., Savchenko, M., Nara, C., & Hagiwara, I. (2016), Investigation for industrialization of the Nojima's pairing origami structure, DETC2016-59415, V05BT07A009. doi: 10.1115/DETC2016-59415.

[33] Yang, Y., Nara, C. & Hagiwara, I. (2017), Energy absorption characteristics of pairing origami structure, papers of the Japan Society of Mechanical Engineers, 83 (845) (in Japanese).

[34] Hallquist, J. O. (2007), LS-DYNA keyword user's manual, LSTC (2007).

[35] Belytschko, T. & C. S. Tsay (1984), Explicit algorithms for the nonlinear dynamics of shells, Computer Methods in Applied Mechanics and Engineering, Vol. 43, pp. 251-276.

[36] Tsuda, M. & Hagiwara, I. (1998), Dynamic-explicit finite element analysis methods for large-deformation quasi-static problems, Transactions of the Japan Society of Mechanical Engineers, Series A, 64 (622), 1548-1555 (in Japanese).

[37] Kitagawa, Y., Hagiwara, I. & Tsuda, M. (1991), Dynamic analysis of thin-walled columns with arbitrary section geometry subjected to axial crushing, Transactions of the Japan Society of Mechanical Engineers, Series A, 57 (537), 1135-1139 (in Japanese).

[38] Kitagawa, Y., Hagiwara, I. &Tsuda, M. (1992), Development of a collapse mode control method for side members in vehicle collisions, SAE 910809 1991 Transaction Section 6, 1101-1107.

[39] Hagiwara, I., Tsuda, M., Kitagawa, Y. & Futamata, T. (1991), Method of determining positions of beads, United States Patent, Patent Number 5048345 (in Japanese).